Molecular Dynamics Simulations of Inwardly Rectifying (Kir) Potassium Channels: A Comparative Study †

5 AUTHORS, INCLUDING:

Shozeb Haider
University College London
141 PUBLICATIONS   4,298 CITATIONS

SEE PROFILE

Syma Khalid
University of Southampton
80 PUBLICATIONS   1,217 CITATIONS

SEE PROFILE

Stephen J Tucker
University of Oxford
106 PUBLICATIONS   4,669 CITATIONS

SEE PROFILE

Molecular Dynamics Simulations of Inwardly Rectifying (Kir) Potassium Channels: A Comparative Study[†]

Shozeb Haider,[‡,§] Syma Khalid,[‡] Stephen J. Tucker,[||] Frances M. Ashcroft,[||] and Mark S. P. Sansom*,[‡]

Department of Biochemistry, University of Oxford, South Parks Road, Oxford OX1 3QU, U.K., and Department of Physiology, Anatomy and Genetics, University of Oxford, Parks Road, Oxford OX1 3PT, U.K.

ABSTRACT: Inward rectifier potassium (Kir) channels regulate cell excitability and transport K^+ ions across membranes. Homotetrameric models of three mammalian Kir channels (Kir1.1, Kir3.1, and Kir6.2) have been generated, using the KirBac3.1 transmembrane and rat Kir3.1 intracellular domain structures as templates. All three models have been explored by 10 ns molecular dynamics simulations in phospholipid bilayers. Analysis of the initial structures revealed conservation of potential lipid interaction residues (Trp/Tyr and Arg/Lys side chains near the lipid headgroup−water interfaces). Examination of the intracellular domains revealed key structural differences between Kir1.1 and Kir6.2 which may explain the difference in channel inhibition by ATP. The behavior of all three models in the MD simulations revealed that they have conformational stability similar to that seen for comparable simulations of, for example, structures derived from cryoelectron microscopy data. Local distortions of the selectivity filter were seen during the simulations, as observed in previous simulations of KirBac and in simulations and structures of KcsA. These may be related to filter gating of the channel. The intracellular hydrophobic gate does not undergo any substantial changes during the simulations and thus remains functionally closed. Analysis of lipid−protein interactions of the Kir models emphasizes the key role of the M0 (or "slide") helix which lies approximately parallel to the bilayer−water interface and forms a link between the transmembrane and intracellular domains of the channel.

Potassium channels (*1*) are dynamic membrane proteins of considerable physiological and biomedical interest. They enable and control the flux of K^+ ion across cell membranes. K channel regulation is accomplished by a conformational change that allows the protein to switch between two alternative (closed vs open) conformations, a process known as gating.

The elucidation of the structures of several K channels (*2*) has shed considerable light on the structural basis of the mechanisms of ion selectivity and permeation (*3−12*). These include the following: KcsA, gated by low pH; MthK, gated by Ca^{2+} ions; KvAP and Kv1.2, gated by transmembrane voltage; and KirBac, for which the gating mechanism remains uncertain (but see refs *13* and *14*). All of these structures share a tetrameric pore-forming domain, in which the monomers surround a central pore. Each subunit contains an M1-P-F-M2 motif (S5-P-F-S6 in Kv channels), where M1 and M2 are transmembrane helices and the short pore helix (P) and extended filter (F) region form a re-entrant loop between the two TM helices.

Inward rectifier (Kir)[1] channels have a relatively simple TM architecture, containing only the M1-P-F-M2 motif. In humans, Kir channels have two main physiological roles: They regulate cell excitability by stabilizing the membrane potential close to the K^+ equilibrium potential, and they are involved in the transport of K^+ across membranes (*15*, *16*). Structures for the intracellular domain of mammalian Kir [Kir3.1 (*17*) and Kir2.1 (*18*)] and for the complete channel (i.e., TM and intracellular domains) of two bacterial Kir homologues [KirBac1.1 at 3.7 Å resolution (*9*) and KirBac3.1 at 2.6 Å resolution (*19*)] have been determined.

In the structures of both KirBac1.1 and KirBac3.1, the overall TM topology is similar to that of the simple bacterial channel KcsA, with the addition of a M0 [or "slide" (*9*)] helix N-terminal to the M1 TM helix. Indeed, KcsA does contain an M0 helix (*20*), but this is not resolved in the X-ray structure of the channel (*3*, *21*). The KirBac channels also have an intracellular (IC) domain consisting mostly of β-sheet, with a fold related to that of the Kir3.1 IC domain.

The KirBac1.1 channel is in a closed (i.e., nonconducting) conformation as the intracellular pore mouth, formed by the crossing point of the C-termini of the M2 helices, is hydrophobic and very narrow (only ~0.05 nm in radius, compared with the 0.133 nm radius of a K^+ ion). KirBac3.1 is thought to be in an intermediate state in its crystal structure

1 Abbreviations: IC, intracellular; Kir, inward rectifier; MD, molecular dynamics; PME, particle mesh Ewald; POPC, palmitoyloleoylphosphatidylcholine; rmsd, root-mean-square deviation; TM, transmembrane.

(*19*), with a pore radius at the intracellular mouth of 0.12 nm. The selectivity filters of both KirBac channels are very similar to that of KcsA, with a succession of five potential K^+ ion binding sites formed by cages of eight oxygen atoms. In Kir channels, it is thought that the IC domain acts as a "gatekeeper", interacting with various possible ligands (*17*, *22−24*) to regulate the conformational state of the TM domain gate.

Potassium channels function in a lipid bilayer environment. There is growing evidence of the importance of protein−lipid interactions in channel structure and function. Thus, bound anionic lipid molecules are present in the crystal structure of KcsA and play a key role in its function (*25−28*). A number of studies have implicated lipids, especially inositol phospholipids (*14*, *18*, *22*, *29−31*) but also other lipid signals (*32*), in the regulation of Kir channels. Indeed, inositol phospholipids may regulate a range of channels, including Kir, Kv7 (*33*), and others (*34*). It is therefore worth exploring in more general terms how Kir channels interact with their lipid environment.

Computer simulations provide a useful approach to exploring the conformational dynamics of membrane proteins in a lipid bilayer environment (*35*). There have been many computational studies of ion channels (see ref *36* for a recent review), which have provided valuable insights into, for example, mechanisms of ion permeation. Homology modeling may be used to extrapolate from structures of bacterial potassium channels (*37*) to explanations of the function of their mammalian homologues. For example, homology models have been used to aid the interpretation of the functional effects of mutations in Kir channels (*24*, *38−41*). Molecular simulations have also been used to explore the nature of both nonspecific and specific interactions of lipids with KcsA (*42−45*).

In this study, we present simulations of homology models of three homotetrameric mammalian Kir channels and focus on the use of such simulations in exploring model stability and integrity and lipid−protein interactions.

METHODS

Model Building of Kir Channels. Sequences were aligned using ClustalX (*46*). Homology models were generated using Modeler version 6.2 (http://salilab.org/modeller/modeller. html) (*47−49*). The model of Kir3.1 (residues 43−270) was based on the crystal structures of a bacterial inwardly rectifying K^+ channel (KirBac3.1) (PDB entry 1XL6) and of the intracellular domain (IC) of the rat Kir3.1 channel (PDB entry 1N9P). The transmembrane (TM) region is highly conserved among Kir channels. Thus, as the level of conservation of residues within the TM regions of KirBac3.1 and rat Kir3.1 is 36%, it was decided that the TM region of the KirBac3.1 would be an appropriate model for the TM segment of Kir3.1. The TM region was modeled as a tetramer with 4-fold symmetry imposed. The crystal structure of the IC domain contains both the N- and C-termini of the Kir3.1 sequence. The spatial orientation of the IC domain with respect to the TM region was obtained by superimposing the conserved residues found in the IC domains of Kir3.1 on the KirBac3.1 structure. Once the orientation had been obtained, the IC domains from Kir3.1 were joined to the modeled TM region by residues that were predicted to be in

loops. The secondary structure predictions for the modeled regions were obtained from PHD (www.cubic.bioc. columbia.edu) and JPRED (www.compbio.dundee.ac.uk). The loops were then subjected to steepest descent energy minimization, while the core model was kept fixed.

Homology models for Kir1.1 (residues 39−369) and Kir6.2 (residues 32−358) were derived from the molecular model generated for Kir3.1. This was possible because of the high degree of sequence similarity exhibited by members of the mammalian inwardly rectifying K^+ channel family (∼44% for both sequences). Several minimization steps were required in the model building process to obtain a low-energy conformation of the models without steric clashes between the side chains. The quality and the stereochemical properties of the models were assessed after each step using PROCHECK version 3.4.4 (*50*).

Molecular Dynamics Simulations. X-ray crystallographic and computational studies of a number of bacterial K^+ channels have indicated that the selectivity filter is stably occupied by a single file of alternating K^+ ions and water molecules (for a recent study see, for example, ref *51*). Thus, in preparation for the simulations, two K^+ ions were placed at positions S1 and S3 and water molecules were placed at positions S0, S2, and S4. The central cavity in the models was solvated using Voidoo and Flood (*52*). The resulting models were then embedded in a POPC bilayer with a thickness of ∼35 Å. The protocol for membrane insertion is described in ref *53*. The system was then solvated with SPC (*54*) water molecules. Counterions were added at random positions within the bulk solvent to neutralize the system. This generated systems of ∼97000 atoms. Before the simulations were conducted, each system was energy minimized using 1000 iterations of steepest descent. The systems were then equilibrated for 0.25 ns by a molecular dynamics run during which the non-H protein atoms were harmonically restrained using a force constant of 1000 kJ mol^{-1} nm^{-2}. During this equilibration process, the solvent molecules and the ions were free to move. After the initial equilibration, all restraints were removed from the protein and each system was subjected to a 10 ns production run.

Molecular dynamics simulations were carried out using GROMACS version 3.1.4 (www.gromacs.org) (*55*) with a modified version of the GROMOS87 (*56*) force field. The simulations employed Berendsen coupling (*57*) to maintain a constant temperature of 300 K and a constant isotropic pressure of 1 bar. The van der Waals interactions were modeled using 6-12 Lennard-Jones potentials with a 13 Å cutoff. Long-range electrostatic interactions were calculated using the particle mesh Ewald method (*58*, *59*), with a cutoff for the real space term of 12 Å. Covalent bonds were constrained using the LINCS algorithm (*60*). The time step employed was 2 fs, and the coordinates were saved every 10 ps for analysis. Analysis of the simulations was carried out using the programs in the GROMACS suite of packages and local scripts. Pore dimensions were evaluated using HOLE (*61*). Molecular graphics images were generated using VMD (*62*) and RasMol (*63*).

RESULTS

Structural Features. Before reporting the results of the simulations, we compare the structural features of the models.
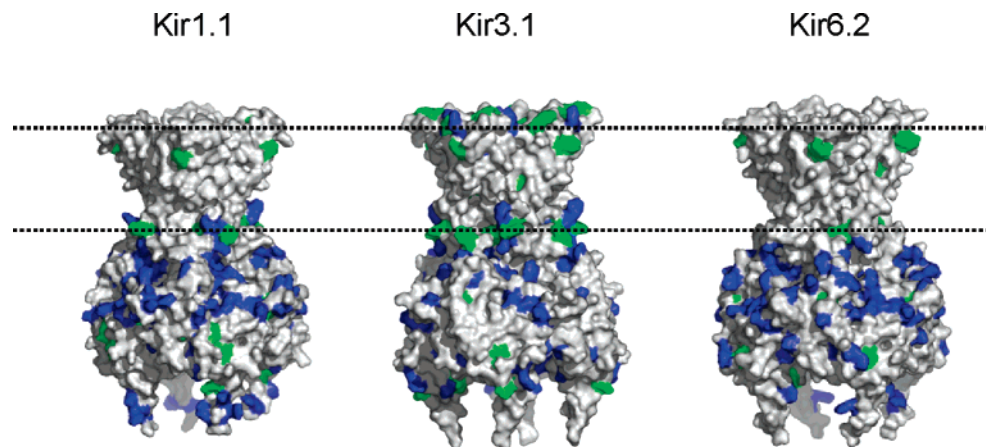
FIGURE 1: Surface representations of the three models, highlighting amphipathic aromatic (Trp and Tyr; green) and basic (Arg and Lys; blue) residues.

It is also valuable to bear in mind the following. (i) Only Kir1.1 and Kir6.2 form homotetramers in vivo, whereas Kir3.1 forms heterotetramers in vivo with Kir3.2 or Kir3.4 (*64*) (although a point mutation of Kir3.1 may form homotetramers in vitro) (*65*). (ii) Kir6.2 in vivo exists in complex with another subunit [the sulfonylurea receptor, SUR (*66*)] and, when expressed as the Kir6.2 heterotetramer (*67*), exhibits gating properties different from those of the native K_{ATP} (i.e., Kir6.2−SUR complex) channel. Thus, the three models span a native homotetramer (Kir1.1), an "artificial" homotetramer (Kir3.1), and a homotetramer (Kir6.2) without its native partner subunit. Visualization of the surface-exposed residues of the three Kir models is informative (see Figure 1). Two features which one would expect in a membrane protein are bands of amphipathic aromatic (i.e., Trp and Tyr) side chains associated with the bilayer−water interface, and the presence of basic side chains just outside of the transmembrane region of the protein surface where they can interact with lipid phosphate groups (see, for example, ref *68* for a discussion of how membrane proteins interact with a bilayer−water interface). All three models show clear bands of Trp and Tyr residues. However, only in Kir3.1 are bands of basic side chains present at both the intracellular and extracellular interfacial regions; in Kir1.1 and Kir6.2, only the intracellular interfacial region contains basic residues. This is perhaps not surprising given the asymmetry of distribution of basic residues seen in membrane proteins in general (*69*).

Since the crystal structure on which the TM domain of the models was based was of a closed state of KirBac3.1, the models are also in a closed conformation, at least as far as the pore is concerned. The intracellular domain conformation is based on that of the Kir3.1 IC domain (*17*) and may also correspond to a closed conformation, although this is less certain than for the TM domain.

There are some differences between the models in the residues that line the central ion conduction pathway. These have been explored by calculating the pore radius profile of the models (Figure 2). The length of the pores of the models (*z*) spans from approximately 20 Å on the intracellular side to approximately −60 Å on the extracellular end of the channel. The pore radius profile and the pore surface reveal a number of constrictions along the ion conduction pathway. All of these constrictions lie within the TM region of the
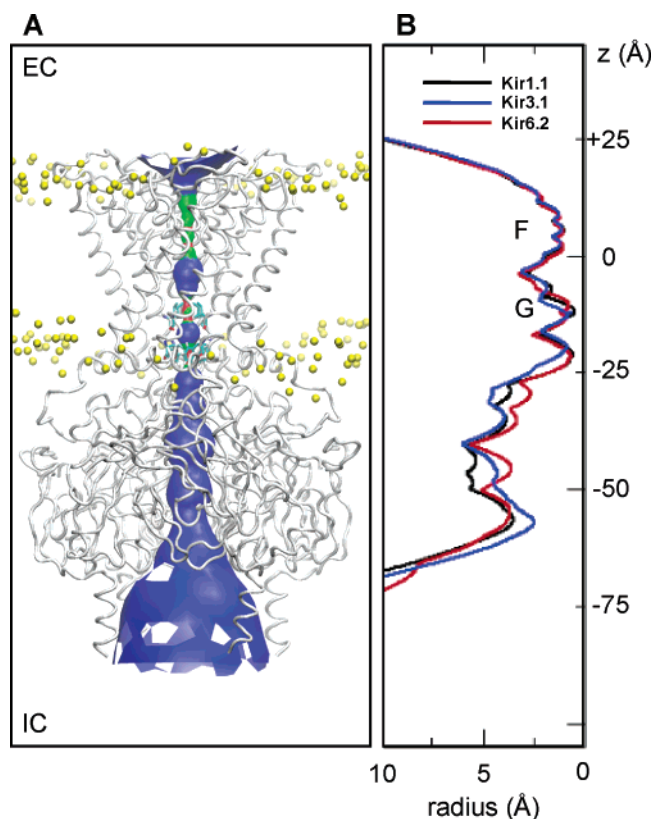

FIGURE 2: (A) Kir model (shown as a gray Cα trace for Kir3.1) in the POPC bilayer. The P atoms of the lipid headgroups are shown as yellow spheres. The pore lining generated using HOLE (*61*) is shown as a red (radius < size of water), green (radius ≈ size of water), and blue (radius > size of water) surface. (B) Comparison of pore radius profiles (black for Kir1.1, blue for Kir3.1, and red for Kir6.2) with the bilayer normal (i.e., *z*) axis aligned to match the structural diagram in panel A.

models. The signature filter sequence is the first most prominent region encountered by the ion when it enters from the extracellular mouth of the channel. The radius at this point is ∼2 Å in all the models. There are two more constriction rings within the TM region where the radius is reduced to less than ∼1 Å. Both of these constrictions are near the intracellular lipid−water interface. These are formed by residues L179 (and to a lesser extent C175) in Kir1.1, by I177 and F181 in Kir3.1, and by L164 and F168 in Kir6.2 (Figure 3). In the context of this model, it is of interest to
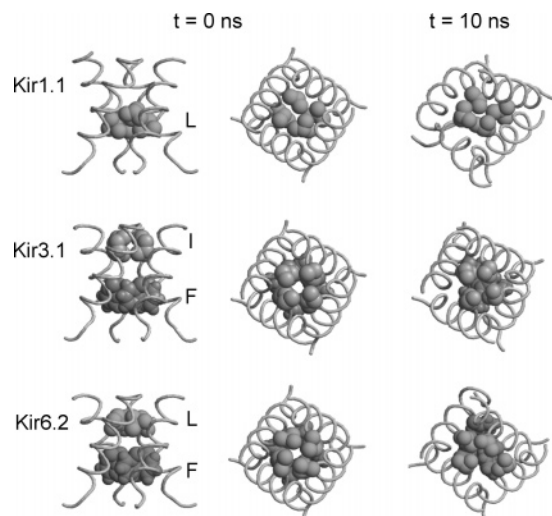
FIGURE 3: Hydrophobic gates shown at the start and end of each simulation. The left column shows the three gates (in the initial, time zero, structures) viewed perpendicular to the pore axis. The center and right columns show the same gates viewed down the pore axis at $t = 0$ and $t = 10$ ns, respectively. Helices are shown as tubes and hydrophobic gate side chains as van der Waals spheres.

note that mutations at L164 (*70*) and F168 (*71*) in Kir6.2 have dramatic effects on gating of the channel.

In each of the simulations, these constrictions do not relax significantly during the simulations. For example, the largest change is for the L164 ring of Kir6.2, where the radius increases from ∼0.4 Å at the start of the simulation to ∼0.8 Å at the end. Thus, in each case, the closed gate is formed by a hydrophobic constriction. Simulations on simple model systems suggest such a hydrophobic constriction can form a closed gate (*72*). These hydrophobic residues lie on the M2 outer helix within each subunit, between the proposed glycine hinge and the helix bundle, and are conserved within the Kir channel family. It is interesting to note that the radius of a solvated K$^+$ ion is ∼4.3 Å while the radius of these rings is ∼1 Å. Thus, these rings are expected to act as effective barriers to ion permeation (*73, 74*). The channel has a broad ion conduction pathway in the intracellular region, and the traversing ion would not have to overcome any other barriers once beyond the TM region.

An approximation to the energetics of K$^+$ ion permeation through the channel along the central pore axis has been obtained by calculating the Born energy profile of a monovalent cation as a function of position along the axis of the central channel pore (*75*). The maximum electrostatic barrier height, associated with the hydrophobic gate, is between ∼50 (Kir6.2) and ∼150 kJ/mol (Kir1.1) (K. Tai et al., manuscript in preparation). In each case, this is more than sufficient to prevent any ions from crossing and thus confirms the closed conformation of the channel models.

Comparison of ATP-Binding Sites. It is worth comparing the potential ATP-binding sites in the initial models prior to simulation, at least in the two (Kir1.1 and Kir6.2) that form homotetramers in vivo. In particular, it is interesting that Kir6.2 exhibits strong inhibition of channel opening by ATP (reviewed in, for example, ref *24*), whereas inhibition of Kir1.1 by ATP is less clear-cut (see, for example, ref *24*). If one compares the potential ATP-binding sites in the Kir1.1. and Kir6.2 models, some important differences emerge. The ATP-binding site on Kir6.2 (*24, 40*) lies in the IC domain
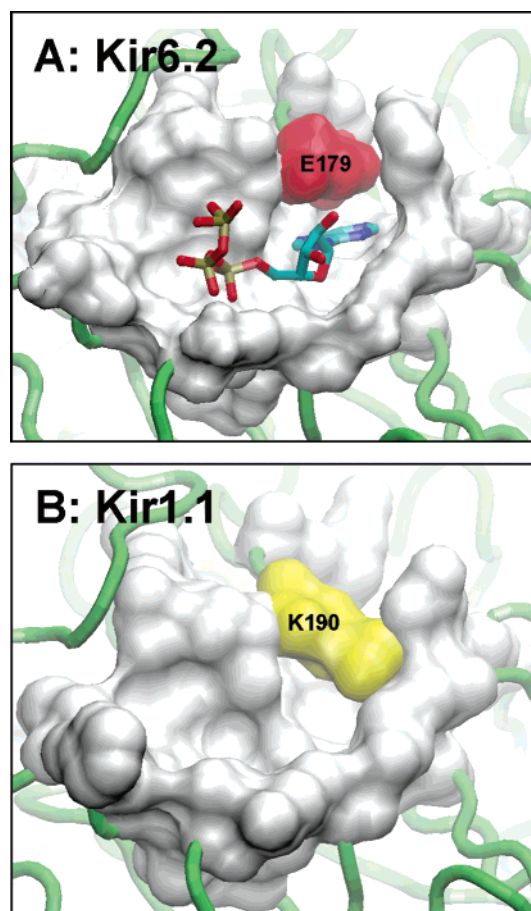

FIGURE 4: Comparison of (A) the ATP-binding site of the Kir6.2 model with (B) the equivalent region in the Kir1.1 model. In panel A, an ATP molecule is shown and the E179 side chain is highlighted in red. In panel B, the K190 residue equivalent to E179 of Kir6.2 is shown highlighted in yellow.

∼17 Å "below" the intracellular leaflet of the membrane. The binding site is sufficient to accommodate the ATP molecule and is arranged in such a manner that the adenine ring and the ribose sugar of the nucleotide are positioned on one side of a β-sheet and the phosphate tail on the other. This effectively results in the separation of charged groups of ATP. The adenine ring is accommodated tightly in a pocket formed by the side chains of E179, T180, L181, and I182 and by the backbone atoms of K38, K39, G40, and R301. The side chain of E179 and the backbone carbonyl atom of R301 form H-bonds to the N6 atom of the adenine ring. If one examines the equivalent residues in Kir1.1, a major difference is that E179 in Kir6.2 is replaced with K190 in Kir1.1 (Figure 4). The presence of a cationic side chain (i.e., K190) close to N6 in the adenine ring may weaken the interaction, as it will be less likely to form a H-bond to the N6 amino group of the ATP than is the anionic side chain of E179. Also, the larger lysine side chain may sterically displace ATP to some extent. Indeed, the E179N and E179M mutations result in a marked decrease in the ATP sensitivity of Kir6.2 (*40*). Furthermore, R50 of Kir6.2 [which is thought to interact with the γ-phosphate of ATP (*40*)] is absent from Kir1.1. Again, this would be expected to weaken the binding of ATP to Kir1.1 relative to the binding to Kir6.2. Indeed, mutation of R50 causes a dramatic decrease in the level of inhibition of Kir6.2 channels by ATP (*76, 77*).
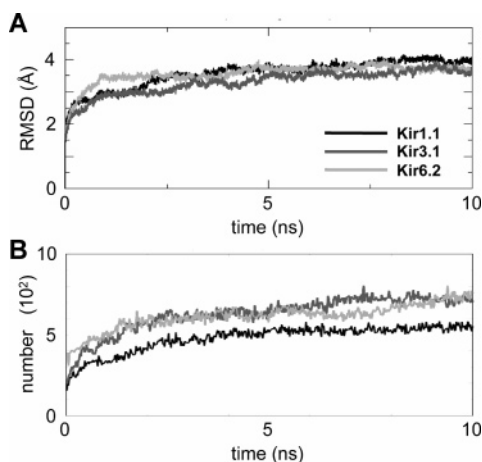
FIGURE 5: (A) Cα rmsds (for all residues) relative to the initial model as a function of time for the three simulations. (B) Number of protein−POPC headgroup interactions (calculated using a 3.5 Å cutoff) as a function of time. For both graphs, the black trace is for Kir1.1, the dark gray trace for Kir3.1, and light gray trace for Kir6.2.

Table 1: Summary of Simulations

simulation	environment	Cα rmsd (all residues) (Å)	Cα rmsd (core TM domain) (Å)	Cα rmsd (core IC domain) (Å)
Kir1.1	214 POPCs, 24 556 waters	3.6	1.3	1.8
Kir3.1	213 POPCs, 23 895 waters	3.3	1.3	1.7
Kir6.2	239 POPCs, 23 845 waters	3.6	1.4	1.9

Conformational Drift and Flexibility. The conformational stability of the models was assessed by carrying out a 10 ns molecular dynamics simulation of each model in a lipid (POPC) bilayer. Previous experience (*38, 78*) suggests that a 10 ns simulation is sufficient to reveal any major conformational instability within the models. Thus, a simple measure of the "quality" of a model can be obtained via the time-dependent root-mean-square deviation (rmsd) of Cα atoms from their position in the initial model after equilibration (Figure 5A). All three models exhibited conformational drifts to similar plateau values of ∼3.5 Å (for Cα atoms of all residues; see Table 1). This degree of drift is comparable to that seen in simulations of cryoelectron microscopy structures (resolution of 3.5 Å) or homology models of aquaporins but slightly higher than that seen in simulations of high-resolution (2.2 Å or better) X-ray structures of membrane proteins (*78*). If one restricts the Cα rmsd calculation to the core regions (i.e., excluding surface loops) of the two domains (TM and IC), the values are much lower (∼1.5 Å), indicating little drift in the core fold of the models, at least on an ∼10 ns time scale.

In addition to the rmsd values, one can also estimate conformational flexibility by calculating the magnitude of the fluctuations as a function of residue number. Such an analysis gives a complete breakdown of the mobility of individual residues (see Figure S1 of the Supporting Information). The greatest fluctuations are all seen in regions which correspond to loops lining the central pore through the IC domain (*41*).

It is important to examine the behavior of key functionally important regions within the channel models during the
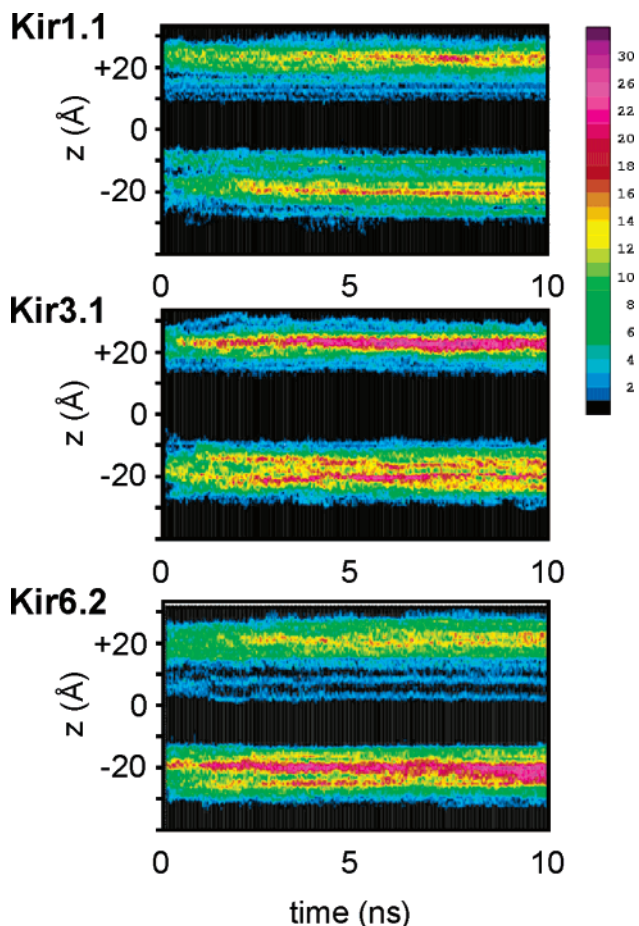

FIGURE 6: Lipid headgroup−protein contacts as a function of location along the bilayer normal (*z*) and time for all three simulations. The color code ranges from deep blue to violet, corresponding to 1−30 contacts at an interatomic distance of <3.5 Å. The lower band of interactions (centered at approximately −20 Å) corresponds to the headgroups of the inner leaflet, and the upper band of interactions (centered at approximately 20 Å) corresponds to the headgroups of the outer leaflet.

simulations. For each of the three models, the selectivity filter remains relatively undistorted, although some "flipping" of peptide bonds in the filter has been observed, in part as a result of movement of the two K$^+$ ions along the selectivity filter during the equilibration phase of the simulation. Thus, in both Kir1.1 and Kir3.1 the Ile carbonyl of the TIGYG filter motif is flipped in two of the four chains after 10 ns, whereas in Kir6.2, the carbonyl of Gly132 (in TIG^{132}FG) is flipped in two chains. Such local distortions of the filter have also been seen in a number of other simulations of K channels (*39, 79−82*) and may be related to the change in conformation of, for example, the KcsA selectivity filter observed in crystal structures determined at low K$^+$ ion concentrations (*21*). As suggested by a recent comparative simulation of KcsA and KirBac (*51*), and by a number of earlier simulations on K channel structures and models (see, for example, refs *79, 83,* and *84*), the filter is relatively invariant in conformation, at least on a 10 ns time scale, if occupied by K$^+$ ions and water molecules in an energetically favorable configuration of alternating cations and water molecules. However, both simulations (*81, 82, 85*) and structural studies [of native KcsA at low K$^+$ concentrations (*21*) and of a filter mutant of KcsA (*12, 86*)] suggest that distortion of the filter may be associated with filter gating
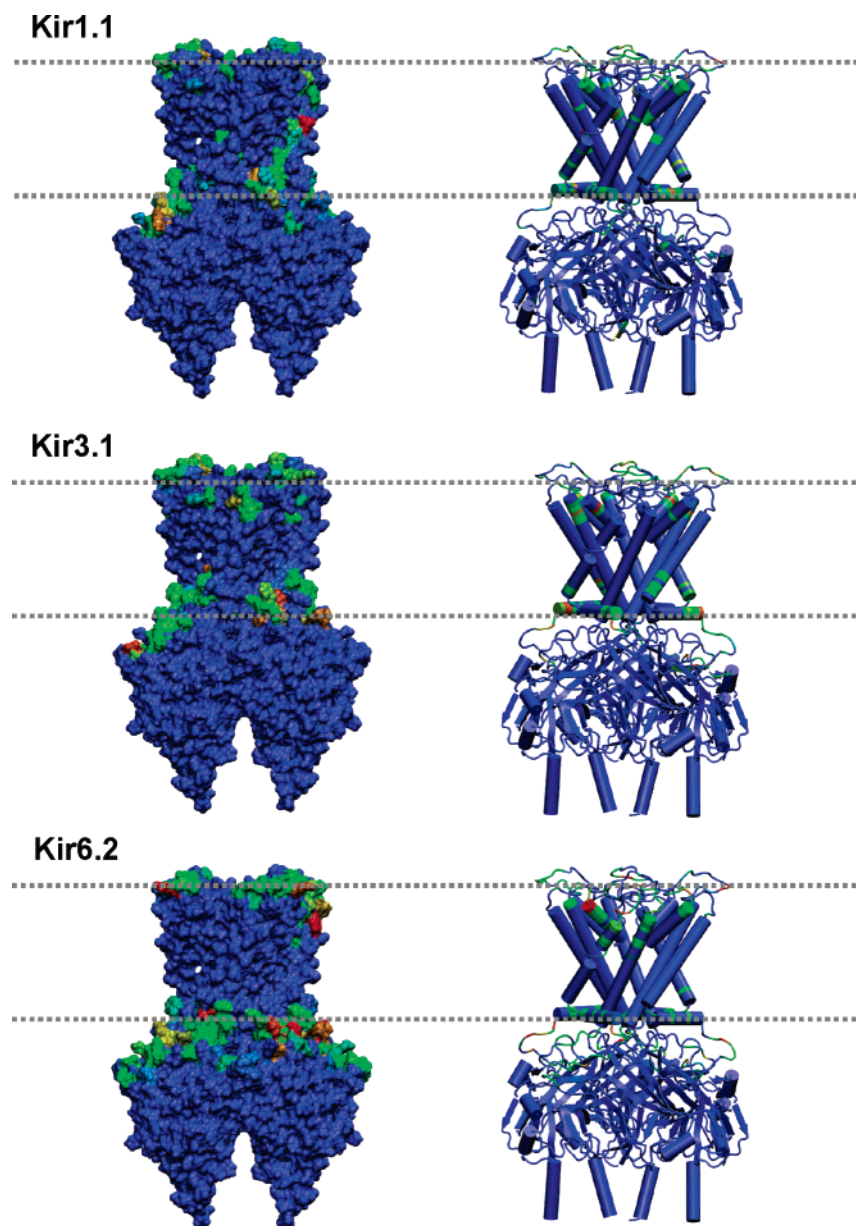
FIGURE 7: Surface (left) and cartoon (right) representations of the three Kir models colored on lipid headgroup−protein contacts using a blue-to-green-to-red scale (i.e., red corresponds to the largest number of contacts). The dashed horizontal lines indicate the approximate locations of the membrane−water interface.

of K channels, although the time scale of the changes in the simulation is faster than that observed experimentally.

The hydrophobic gate region of all three models remains closed over the duration of the simulations, as might be anticipated. Although some local distortion of the hydrophobic gating rings occurs (Figure 3), the pore radii at the gates before (∼0.4 Å for Kir1.1, ∼0.8 Å for Kir3.1, and ∼0.4 Å for Kir6.2) and after (∼0.4 Å for Kir1.1, ∼0.5 Å for Kir3.1, and ∼0.8 Å for Kir6.2) simulations are such that a significant hydrophobic barrier will be present.

Lipid−Protein Interactions. As mentioned above, a number of studies have indicated the importance of channel−lipid interactions in the regulation of Kir (*14, 18, 22, 29−32, 34*) and other [e.g., KcsA (*25−28*) and KvAP (*87*)] potassium channels. It is therefore of some interest to explore the interactions of the Kir channel models with their lipid bilayer environments, and especially with the lipid headgroups.

The total numbers of lipid headgroup−protein interactions (defined as an interatomic distance of ≤3.5 Å) were measured as a function of time (Figure 5B). It can be seen that the total number of contacts increases during the first ∼2.5 ns of each simulation and then plateaus. The total number of contacts was a little lower for Kir1.1 than for the other two models, but otherwise, the overall behavior of the three systems was very similar. For the intracellular interface, this reflects fewer surface-exposed aromatic (Trp and Tyr) residues and for the extracellular interface fewer exposed basic residues for Kir1.1 than for Kir3.1 and Kir6.2 (see Figure 1). A more detailed analysis of the buildup with respect to time of the lipid protein interactions is provided in Figure 6, where contour plots of the number of contacts between lipid headgroup and proteins atoms is shown. The results reveal the presence of two broad bands of interactions (>10 Å wide) corresponding to the two membrane−water interfaces. The widths of the interaction bands correspond
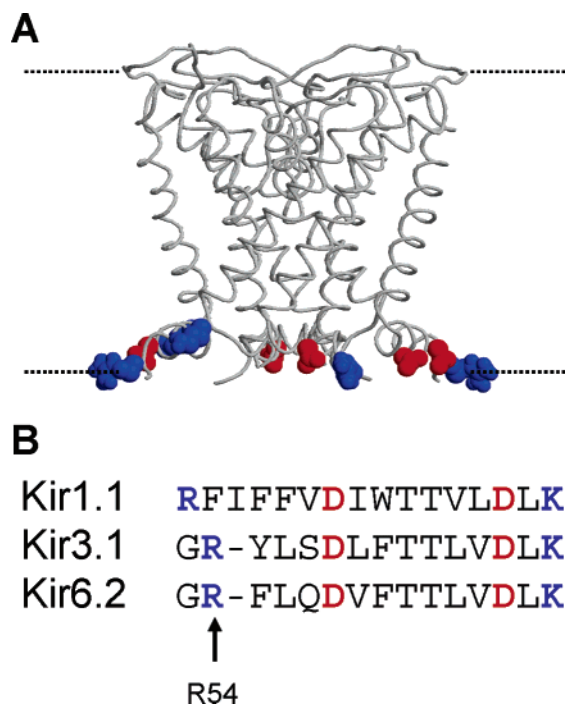
FIGURE 8: (A) Diagram of the transmembrane domain of Kir6.2, showing those side chains of the M0 helix which form the most contacts to lipid headgroups as a space-filling model (red for Asp and blue for Arg and Lys). (B) Alignment of the M0 sequences of the three Kir species, with the residues shown in panel A highlighted. Residue R54 of Kir6.2 (see the text) is denoted with an arrow.

to the thicknesses of the interfacial (i.e., lipids headgroups and water molecules) seen in other simulations and also as measured by combined X-ray and neutron experiments (*88*).

One may analyze the number of contacts further by considering the contributions made by individual protein residues (Figure 7). Such analysis reveals that the major contact residues lie in (i) the extracellular loops, (ii) the extracellular ends of the TM helices [a region implicated in specific anionic lipids binding sites in KcsA (*44*)], (iii) the M0 helix, i.e., the short slide (*9*) helix which is just before the first TM helix and lies close to the intracellular membrane−water interface, and (iv) the surface of the intracellular domain facing the lipid headgroups. Note that the latter region has been implicated in ATP and PIP$_2$ binding in Kir6.2 (*89*−*91*).

It should be noted that the M0 helix may move during gating (*9*, *92*). Thus, the nature of lipid−protein contacts involving M0 may play a role in the control of gating. The contacts of the side chains of the M0 helix of, for example, Kir6.2 with the lipid headgroups were therefore examined in more detail (Figure 8). This reveals that a pattern of conserved basic (Arg/Lys) and acidic (Asp) side chains forms frequent contacts with the headgroups. This is of some interest given the proposed role of the M0 helix in the gating mechanism of Kir channels (*9*), and the modulation of Kir channel gating by lipids (see above). For example, one of the residues in M0 of Kir6.2 that interacts with lipid headgroups is R54. This residue has been implicated in interactions of the channel with PIP$_2$ (*30*). Thus, the M0 helix is perhaps uniquely poised to integrate interactions with lipid headgroups and with the residues of the regulatory IC domain.

CONCLUSIONS

From these simulations, it would seem that homology modeling combined with MD simulations can yield candidate structures which promise some insight into mammalian Kir channels. In particular, the relative stability of the three different models in the simulations is comparable to, for example, that of low-resolution EM structures (*78*), reinforcing the suggestion that they are reasonable representations of the true structures of the channels. Indeed, recent studies of homology modeling of membrane proteins (*93*) suggest that acceptable models (i.e., with Cα rmsd values with respect to the native of ≤2 Å in the transmembrane regions) may be obtained for levels of template sequence identity of ≥30%.

One of the features clearly conserved between the models is the hydrophobic gate (*94*) region of the pores. Examination of these gates at the start and end of the simulations suggests that they remain closed, as might be expected given the time scale of the simulations and the fact that the initial models were derived by using a closed channel structure as the template for the TM domain.

The simulations based on the models have been of particular use in yielding insights into the nature of Kir channel−lipid interactions. In particular, the results emphasize the importance of the M0 helix and of the loops lining the TM and IC domains in forming interactions with the headgroups of the lipids of the intracellular leaflet of the lipid bilayer. This is of particular interest given the accumulating evidence of the role of specific intracellular leaflet lipids in modulating Kir channel activity (*14*, *90*, *91*).

It is important to consider the limitations of this study. The simulations are relatively short and will only incompletely sample protein motions (*95*). However, the comparison between simulations of three related proteins can help to overcome this limitation to some extent. It is also known that the use of PME for long-range electrostatics interactions is at best an approximation and can lead to possible artifacts (*96*). In terms of electrostatic interactions, it would also be of interest to explore the effect of changing the ionization states of key residues (*97*) and of changing the concentration of K$^+$ to a higher value (e.g., 0.5 M). Perhaps a more serious approximation in the context of this study is the use of a simple lipid species (POPC). A pressing future extension to this study is to use simulations to explore the interactions of Kir channels with more complex lipids, including phosphoinositides.

ACKNOWLEDGMENT

SUPPORTING INFORMATION AVAILABLE

Analysis of the Cα atom root-mean-square fluctuation (rmsf) as a function of residue number for the three simulations. This material is available free of charge via the Internet at http://pubs.acs.org.

REFERENCES

1. Yellen, G. (2002) The voltage-gated potassium channels and their relatives, *Nature 419*, 35−42.

2. Mackinnon, R. (2003) Potassium channels, *FEBS Lett. 555*, 62–65.

3. Doyle, D. A., Cabral, J. M., Pfuetzner, R. A., Kuo, A., Gulbis, J. M., Cohen, S. L., Cahit, B. T., and MacKinnon, R. (1998) The structure of the potassium channel: Molecular basis of K⁺ conduction and selectivity, *Science 280*, 69–77.

4. Morais-Cabral, J. H., Zhou, Y., and MacKinnon, R. (2001) Energetic optimization of ion conduction by the K⁺ selectvity filter, *Nature 414*, 37–42.

5. Zhou, Y., and MacKinnon, R. (2003) The occupancy of ions in the K⁺ selectivity filter: Charge balance and coupling of ion binding to a protein conformational change underlie high conduction rates, *J. Mol. Biol. 333*, 965–975.

6. Jiang, Y., Lee, A., Chen, J., Cadene, M., Chait, B. T., and MacKinnon, R. (2002) Crystal structure and mechanism of a calcium-gated potassium channel, *Nature 417*, 515–522.

7. Jiang, Y., Lee, A., Chen, J., Cadene, M., Chait, B. T., and MacKinnon, R. (2002) The open pore conformation of potassium channels, *Nature 417*, 523–526.

8. Jiang, Y., Lee, A., Chen, J., Ruta, V., Cadene, M., Chait, B. T., and Mackinnon, R. (2003) X-ray structure of a voltage-dependent K⁺ channel, *Nature 423*, 33–41.

9. Kuo, A., Gulbis, J. M., Antcliff, J. F., Rahman, T., Lowe, E. D., Zimmer, J., Cuthbertson, J., Ashcroft, F. M., Ezaki, T., and Doyle, D. A. (2003) Crystal structure of the potassium channel KirBac1.1 in the closed state, *Science 300*, 1922–1926.

10. Long, S. B., Campbell, E. B., and MacKinnon, R. (2005) Crystal structure of a mammalian voltage-dependent Shaker family K⁺ channel, *Science 309*, 897–902.

11. Shi, N., Ye, S., Alam, A., Chen, L., and Jiang, Y. (2006) Atomic structure of a Na⁺- and K⁺-conducting channel, *Nature 440*, 570–574.

12. Cordero-Morales, J. F., Cuello, L. G., Zhao, Y. X., Jogini, V., Cortes, D. M., Roux, B., and Perozo, E. (2006) Molecular determinants of gating at the potassium-channel selectivity filter, *Nat. Struct. Mol. Biol. 13*, 311–318.

13. Enkvetchakul, D., Bhattacharyya, J., Jeliazkova, I., Groesbeck, D. K., Cukras, C. A., and Nichols, C. G. (2004) Functional characterization of a prokaryotic Kir channel, *J. Biol. Chem. 279*, 47076–47080.

14. Enkvetchakul, D., Jeliazkova, I., and Nichols, C. G. (2005) Direct modulation of Kir channel gating by membrane phosphatidyli-nositol 4,5-bisphosphate, *J. Biol. Chem. 280*, 35785–35788.

15. Nichols, C. G., and Lopatin, A. N. (1997) Inward rectifier potassium channels, *Annu. Rev. Physiol. 59*, 171–191.

16. Reimann, F., and Ashcroft, F. M. (1999) Inwardly rectifying potassium channels, *Curr. Opin. Cell Biol. 11*, 503–508.

17. Nishida, M., and MacKinnon, R. (2002) Structural basis of inward rectification: Cytoplasmic pore of the G protein-gated inward rectifier GIRK1 at 1.8 Å resolution, *Cell 111*, 957–965.

18. Pegan, S., Arrabit, C., Zhou, W., Kwiatkowski, W., Collins, A., Slesinger, P. A., and Choe, S. (2005) Cytoplasmic domain structures of Kir2.1 and Kir3.1 show sites for modulating gating and rectification, *Nat. Neurosci. 8*, 279–287.

19. Gulbis, J. M., Kuo, A., Smith, B., Doyle, D. A., Edwards, A., Arrowsmith, C., and Sundstrom, M. (2005) Two intermediate gating state crystal structures of the KirBac3.1 K⁺ channel, manuscript to be published.

20. Cortes, D. M., Cuello, L. G., and Perozo, E. (2001) Molecular architecture of full-length KcsA: Role of cytoplasmic domains in ion permeation and activation gating, *J. Gen. Physiol. 117*, 165–180.

21. Zhou, Y., Morais-Cabral, J. H., Kaufman, A., and MacKinnon, R. (2001) Chemistry of ion coordination and hydration revealed by a K⁺ channel-Fab complex at 2.0 Å resolution, *Nature 414*, 43–48.

22. Du, X. O., Zhang, H. L., Lopes, C., Mirshahi, T., Rohacs, T., and Logothetis, D. E. (2004) Characteristic interactions with phos-phatidylinositol 4,5- bisphosphate determine regulation of Kir channels by diverse modulators, *J. Biol. Chem. 279*, 37271–37281.

23. Dabrowski, M., Tarasov, A., and Ashcroft, F. M. (2004) Mapping the architecture of the ATP-binding site of the K-ATP channel subunit Kir6.2, *J. Physiol. 557*, 347–354.

24. Trapp, S., Haider, S., Sansom, M. S. P., Ashcroft, F. M., and Jones, P. (2003) Identification of residues contributing to the ATP binding site of Kir6.2, *EMBO J. 22*, 2903–2912.

25. Valiyaveetil, F. I., Zhou, Y., and MacKinnon, R. (2002) Lipids in the structure, folding and function of the KcsA channel, *Biochemistry 41*, 10771–10777.

26. Demmers, J. A. A., van Dalen, A., de Kruijff, B., Heck, A. J. R., and Killian, J. A. (2003) Interaction of K channel KcsA with membrane phospholipids as studied by ESI mass spectrometry, *FEBS Lett. 541*, 28–32.

27. Williamson, I. M., Alvis, S. J., East, J. M., and Lee, A. G. (2003) The potassium channel KcsA and its interaction with the lipid bilayer, *Cell. Mol. Life Sci. 60*, 1581–1590.

28. Marius, P., Alvis, S. J., East, J. M., and Lee, A. G. (2005) The interfacial lipid binding site on the potassium channel KcsA is specific for anionic phospholipids, *Biophys. J. 89*, 4081–4089.

29. Lopes, C. M. B., Zhang, H. L., Rohacs, T., Jin, T. H., Yang, J., and Logothetis, D. E. (2002) Alterations in conserved Kir channel-PIP2 interactions underlie channelopathies, *Neuron 34*, 933–944.

30. Schulze, D., Krauter, T., Fritzenschaft, H., Soom, M., and Baukrowitz, T. (2003) Phosphatidylinositol 4,5-bisphosphate (PIP2) modulation of ATP and pH sensitivity in Kir channels. A tale of an active and a silent PIP2 site in the N terminus, *J. Biol. Chem. 278*, 10500–10505.

31. Lin, C. W., Yan, F. F., Shimamura, S., Barg, S., and Shyng, S. L. (2005) Membrane phosphoinositides control insulin secretion through their effects on ATP-sensitive K⁺ channel activity, *Diabetes 54*, 2852–2858.

32. Ochi, R., Momose, Y., Oyama, K., and Giles, W. R. (2006) Sphingosine-1-phosphate effects on guinea pig atrial myocytes: Alterations in action potentials and K⁺ currents, *Cardiovasc. Res. 70*, 88–96.

33. Li, Y., Gamper, N., Hilgemann, D. W., and Shapiro, M. S. (2005) Regulation of Kv7 (KCNQ) K⁺ channel open probability by phosphatidylinositol 4,5-bisphosphate, *J. Neurosci. 25*, 9825–9835.

34. Suh, B. C., and Hille, B. (2005) Regulation of ion channels by phosphatidylinositol 4,5-bisphosphate, *Curr. Opin. Neurobiol. 15*, 370–378.

35. Ash, W. L., Zlomislic, M. R., Oloo, E. O., and Tieleman, D. P. (2004) Computer simulations of membrane proteins, *Biochim. Biophys. Acta 1666*, 158–189.

36. Roux, B., and Schulten, K. (2004) Computational studies of membrane channels, *Structure 12*, 1343–1351.

37. Gulbis, J. M., and Doyle, D. A. (2004) Potassium channel structures: Do they conform? *Curr. Opin. Struct. Biol. 14*, 440–446.

38. Capener, C. E., Shrivastava, I. H., Ranatunga, K. M., Forrest, L. R., Smith, G. R., and Sansom, M. S. P. (2000) Homology modelling and molecular dynamics simulation studies of an inward rectifier potassium channel, *Biophys. J. 78*, 2929–2942.

39. Capener, C. E., Proks, P., Ashcroft, F. M., and Sansom, M. S. P. (2003) Filter flexibility in a mammalian K channel: Models and simulations of Kir6.2 mutants, *Biophys. J. 84*, 2345–2356.

40. Antcliffe, J. F., Haider, S., Proks, P., Sansom, M. S. P., and Ashcroft, F. M. (2005) Functional analysis of a structural model of the ATP-binding site of the K$_{ATP}$ channel Kir6.2 subunit, *EMBO J. 24*, 229–239.

41. Haider, S., Antcliff, J. F., Proks, P., Sansom, M. S. P., and Ashcroft, F. M. (2005) Focus on Kir6.2: A key component of the ATP-sensitive potassium channel, *J. Mol. Cell. Cardiol. 38*, 927–936.

42. Domene, C., Bond, P. J., Deol, S. S., and Sansom, M. S. P. (2003) Lipid-protein interactions and the membrane/water interfacial region, *J. Am. Chem. Soc. 125*, 14966–14967.

43. Deol, S. S., Bond, P. J., Domene, C., and Sansom, M. S. P. (2004) Lipid-protein interactions of integral membrane proteins: A comparative simulation study, *Biophys. J. 87*, 3737–3749.

44. Deol, S. S., Domene, C., Bond, P. J., and Sansom, M. S. P. (2006) Anionic phospholipids interactions with the potassium channel KcsA: Simulation studies, *Biophys. J. 90*, 822–830.

45. Sansom, M. S. P., Bond, P. J., Deol, S. D., Grottesi, A., Haider, S., and Sands, Z. A. (2005) Molecular simulations and lipid/protein interactions: Potassium channels and other membrane proteins, *Biochem. Soc. Trans. 33*, 916–920.

46. Jeanmougin, F., Thompson, J. D., Gouy, M., Higgins, D. G., and Gibson, T. J. (1998) Multiple sequence alignment with Clustal X, *Trends Biochem. Sci. 23*, 403–405.

47. Sali, A., and Blundell, T. L. (1993) Comparative protein modeling by satisfaction of spatial restraints, *J. Mol. Biol. 234*, 779–815.

48. Fiser, A., Kinh Gian Do, R., and Sali, A. (2000) Modeling of loops in protein structures, *Protein Sci. 9*, 1753–1773.

49. Marti-Renom, M. A., Stuart, A., Fiser, A., Sanchez, R., Melo, F., and Sali, A. (2000) Comparative protein structure modelling of genes and genomes, *Annu. Rev. Biophys. Biomol. Struct. 29*, 291−325.

50. Laskowski, R. A., Macarthur, M. W., Moss, D. S., and Thornton, J. M. (1993) Procheck: A program to the stereochemical quality of protein structures, *J. Appl. Crystallogr. 26*, 283−291.

51. Hellgren, M., Sandberg, L., and Edholm, O. (2006) A comparison between two prokaryotic potassium channels (KirBac1.1 and KcsA) in a molecular dynamics (MD) simulation study, *Biophys. Chem. 120*, 1−9.

52. Kleywegt, G. J., and Jones, T. A. (1994) Detection, delineation, measurement and display of cavities in macromolecular structures, *Acta Crystallogr. D50*, 178−185.

53. Faraldo-Gómez, J. D., Smith, G. R., and Sansom, M. S. P. (2002) Setup and optimisation of membrane protein simulations, *Eur. Biophys. J. 31*, 217−227.

54. Hermans, J., Berendsen, H. J. C., van Gunsteren, W. F., and Postma, J. P. M. (1984) A consistent empirical potential for water-protein interactions, *Biopolymers 23*, 1513−1518.

55. Lindahl, E., Hess, B., and van der Spoel, D. (2001) GROMACS 3.0: A package for molecular simulation and trajectory analysis, *J. Mol. Model. 7*, 306−317.

56. van Gunsteren, W. F., and Berendsen, H. J. C. (1987) *Gromos-87 manual*, Biomos BV, Groningen, The Netherlands.

57. Berendsen, H. J. C., Postma, J. P. M., van Gunsteren, W. F., DiNola, A., and Haak, J. R. (1984) Molecular dynamics with coupling to an external bath, *J. Chem. Phys. 81*, 3684−3690.

58. Darden, T., York, D., and Pedersen, L. (1993) Particle mesh Ewald: An N.log(N) method for Ewald sums in large systems, *J. Chem. Phys. 98*, 10089−10092.

59. Essmann, U., Perera, L., Berkowitz, M. L., Darden, T., Lee, H., and Pedersen, L. G. (1995) A smooth particle mesh Ewald method, *J. Chem. Phys. 103*, 8577−8593.

60. Hess, B., Bekker, H., Berendsen, H. J. C., and Fraaije, J. G. E. M. (1997) LINCS: A linear constraint solver for molecular simulations, *J. Comput. Chem. 18*, 1463−1472.

61. Smart, O. S., Neduvelil, J. G., Wang, X., Wallace, B. A., and Sansom, M. S. P. (1996) Hole: A program for the analysis of the pore dimensions of ion channel structural models, *J. Mol. Graphics 14*, 354−360.

62. Humphrey, W., Dalke, A., and Schulten, K. (1996) VMD: Visual Molecular Dynamics, *J. Mol. Graphics 14*, 33−38.

63. Sayle, R. A., and Milner-White, E. J. (1995) RasMol: Biomolecular graphics for all, *Trends Biochem. Sci. 20*, 374−376.

64. Ma, D., Zerangue, N., Raab-Graham, K., Fried, S. R., Jan, Y. N., and Jan, L. Y. (2002) Diverse trafficking patterns due to multiple traffic motifs in G protein-activated inwardly rectifying potassium channels from brain and heart, *Neuron 33*, 715−729.

65. Vivaudou, M., Chan, K. W., Sui, J. L., Jan, L. Y., Reuveny, E., and Logothetis, D. E. (1997) Probing the G-protein regulation of GIRK1 and GIRK4, the two subunits of the KACh channel, using functional homomeric mutants, *J. Biol. Chem. 272*, 31553−31560.

66. Mikhailov, M. V., Campbell, J., de Wet, H., Shimomura, K., Zadek, B., Collins, R. F., Sansom, M. S. P., Ford, R. C., and Ashcroft, F. M. (2005) 3-D structural and functional characterization of the purified KATP channel complex Kir6.2-SUR1, *EMBO J. 24*, 4166−4175.

67. Tucker, S. J., Gribble, F. M., Zhao, C., Trapp, S., and Ashcroft, F. M. (1997) Truncation of Kir6.2 produces ATP-sensitive K^+ channels in the absence of the sulphonylurea receptor, *Nature 387*, 179−183.

68. Killian, J. A., and von Heijne, G. (2000) How proteins adapt to a membrane-water interface, *Trends Biochem. Sci. 25*, 429−434.

69. Nilsson, J., Persson, B., and von Heijne, G. (2005) Comparative analysis of amino acid distributions in integral membrane proteins from 107 genomes, *Proteins: Struct., Funct., Bioinf. 60*, 606−616.

70. Enkvetchakul, D., Loussouarn, G., Makhina, E., Shyng, S. L., and Nichols, C. G. (2000) The kinetic and physical basis of K(ATP) channel gating: Toward a unified molecular understanding, *Biophys. J. 78*, 2334−2348.

71. Rojas, A., Wu, J., Wang, R., and Jiang, C. (2007) Gating of the ATP-sensitive K^+ channel by a pore-lining phenylalanine residue, *Biochim. Biophys. Acta 1768*, 39−51.

72. Beckstein, O., Biggin, P. C., and Sansom, M. S. P. (2001) A hydrophobic gating mechanism for nanopores, *J. Phys. Chem. B 105*, 12902−12905.

73. Beckstein, O., Biggin, P. C., Bond, P. J., Bright, J. N., Domene, C., Grottesi, A., Holyoake, J., and Sansom, M. S. P. (2003) Ion channel gating: Insights via molecular simulations, *FEBS Lett. 555*, 85−90.

74. Beckstein, O., Tai, K., and Sansom, M. S. P. (2004) Not ions alone: Barriers to ion permeation in nanopores and channels, *J. Am. Chem. Soc. 126*, 14694−14695.

75. Jogini, V., and Roux, B. (2005) Electrostatics of the intracellular vestibule of K^+ channels, *J. Mol. Biol. 354*, 272−288.

76. Proks, P., Gribble, F. M., Adhikari, R., Tucker, S. J., and Ashcroft, F. M. (1998) Involvement of the N-terminus of Kir6.2 in the inhibition of the K_{ATP} channel by ATP, *J. Physiol. 514*, 19−25.

77. Shimomura, K., Girard, C. A. J., Proks, P., Nazim, J., Lippiat, J. D., Cerutti, F., Lorini, R., Ellard, S., Hattersely, A., Barbetti, F., and Ashcroft, F. M. (2006) Mutations at the same residue (R50) of Kir6.2 (KCNJ11) produce different functional effects, *Diabetes 55*, 1705−1712.

78. Law, R. J., Capener, C., Baaden, M., Bond, P. J., Campbell, J., Patargias, G., Arinaminpathy, Y., and Sansom, M. S. P. (2005) Membrane protein structure quality in molecular dynamics simulation, *J. Mol. Graphics Modell. 24*, 157−165.

79. Bernèche, S., and Roux, B. (2000) Molecular dynamics of the KcsA K^+ channel in a bilayer membrane, *Biophys. J. 78*, 2900−2917.

80. Holyoake, J., Domene, C., Bright, J. N., and Sansom, M. S. P. (2003) KcsA closed and open: Modelling and simulation studies, *Eur. Biophys. J. 33*, 238−246.

81. Domene, C., Grottesi, A., and Sansom, M. S. P. (2004) Filter flexibility and distortion in a bacterial inward rectifier K^+ channel: Simulation studies of KirBac1.1, *Biophys. J. 87*, 256−267.

82. Bernèche, S., and Roux, B. (2005) A gate in the selectivity filter of potassium channels, *Structure 13*, 591−600.

83. Guidoni, L., Torre, V., and Carloni, P. (1999) Potassium and sodium binding in the outer mouth of the K^+ channel, *Biochemistry 38*, 8599−8604.

84. Shrivastava, I. H., and Sansom, M. S. P. (2000) Simulations of ion permeation through a potassium channel: Molecular dynamics of KcsA in a phospholipid bilayer, *Biophys. J. 78*, 557−570.

85. Capener, C. E., and Sansom, M. S. P. (2002) MD Simulations of a K channel model: Sensitivity to changes in ions, waters and membrane environment, *J. Phys. Chem. B 106*, 4543−4551.

86. Cordero-Morales, J. F., Cuello, L. G., and Perozo, E. (2006) Voltage-dependent gating at the KcsA selectivity filter, *Nat. Struct. Mol. Biol. 13*, 319−322.

87. Schmidt, D., Jiang, Q. X., and MacKinnon, R. (2006) Phospholipids and the origin of cationic gating charges in voltage sensors, *Nature 444*, 775−779.

88. Wiener, M. C., and White, S. H. (1992) Structure of a fluid dioleoylphosphatidylcholine bilayer determined by joint refinement of X-ray and neutron diffraction data. III. Complete structure, *Biophys. J. 61*, 434−447.

89. Ribalet, B., John, S. A., Xie, L. H., and Weiss, J. N. (2006) ATP-sensitive K^+ channels: Regulation of bursting by the sulphonylurea receptor, PIP2 and regions of Kir6.2, *J. Physiol. 571*, 303−317.

90. Fox, J. E. M., Nichols, C. G., and Light, P. E. (2004) Activation of adenosine triphosphate-sensitive potassium channels by acyl coenzyme A esters involves multiple phosphatidylinositol 4,5-bisphosphate-interacting residues, *Mol. Endocrinol. 18*, 679−686.

91. Schulze, D., Rapedius, M., Krauter, T., and Baukrowitz, T. (2003) Long-chain acyl-CoA esters and phosphatidylinositol phosphates modulate ATP inhibition of K-ATP channels by the same mechanism, *J. Physiol. 552*, 357−367.

92. Kuo, A. L., Domene, C., Johnson, L. N., Doyle, D. A., and Venien-Bryan, C. (2005) Two different conformational states of the KirBac3.1 potassium channel revealed by electron crystallography, *Structure 13*, 1463−1472.

93. Forrest, L. R., Tang, C. L., and Honig, B. (2006) On the accuracy of homology modeling and sequence alignment methods applied to membrane proteins, *Biophys. J. 91*, 508−517.

94. Beckstein, O., and Sansom, M. S. P. (2004) The influence of geometry, surface character and flexibility on the permeation of ions and water through biological pores, *Phys. Biol. 1*, 42−52.

95. Faraldo-Gómez, J. D., Forrest, L. R., Baaden, M., Bond, P. J., Domene, C., Patargias, G., Cuthbertson, J., and Sansom, M. S. P. (2004) Conformational sampling and dynamics of membrane proteins from 10-nanosecond computer simulations, *Proteins: Struct., Funct., Bioinf. 57*, 783−791.

96. Kastenholz, M. A., and Hünenberger, P. H. (2004) Influence of artificial periodicity and ionic strength in molecular dynamics simulations of charged biomolecules employing lattice-sum methods, *J. Phys. Chem. B 108*, 774−788.

97. Varma, S., Chiu, S. W., and Jakobsson, E. (2006) The influence of amino acid protonation states on molecular dynamics simulations of the bacterial porin OmpF, *Biophys. J. 90*, 112−123.

BI062210F

Supplementary Material

Molecular Dynamics Simulations of Inwardly Rectifying (Kir) Potassium Channels: A Comparative Study

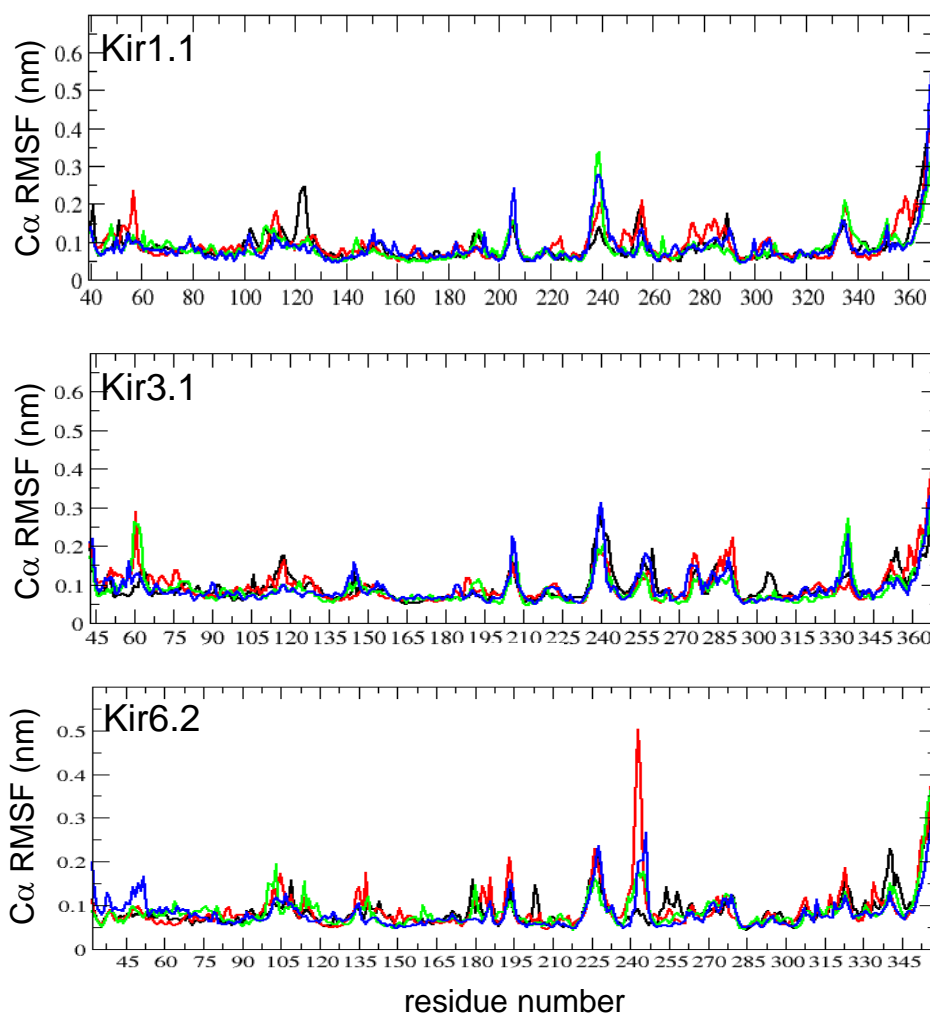*Shozeb Haider, Syma Khalid, Stephen Tucker, Frances M. Ashcroft, & Mark S.P. Sansom*

Figure S1

Cα atom root mean square fluctuation (RMSF) as a function of residue number for the three simulations. In each case, the four differently coloured lines correspond to the four subunits of the channel protein.